RSC Advances

PAPER

View Article Online
View Journal | View Issue

Cite this: *RSC Adv.*, 2022, **12**, 23801

A simple electrochemical aptasensor for saxitoxin detection†

Weixian Zheng, Xinyu Liu, Qianwen Li, Zuju Shu, Zhongbo Li * and Lijun Zhang *

In this study, a simple electrochemical aptasensor for saxitoxin (STX) detection was developed based on a short anti-STX aptamer with a methylene blue (MB) incorporated at the 3′-end. The aptamer was immobilized on the surface of gold electrode and served as the recognition element. The aptasensor was successfully used as a highly selective and sensitive biosensor for STX detection because of the selection of aptamer along with the excellent electrocatalytical properties of MB. With the increase of the dynamic concentration of STX from 1 nM to 1 μM, the aptasensor exhibited a sensitivity with a peak current change of 2.92 μA per decade and a low detection limit of 1 nM. In addition, the aptasensor demonstrated excellent selectivity to STX, which prevented the interferences from neo-STX, okadaic acid and common metal ions. Using the proposed principle, several other aptasensors with improved performance can be constructed *via* the modification of the electrochemical sensor with appropriate aptamers.

Received 15th June 2022
Accepted 14th August 2022

DOI: 10.1039/d2ra03690h

rsc.li/rsc-advances

1. Introduction

Saxitoxin (STX), one of the paralytic shellfish poisons (PSP) and the most poisonous marine biotoxin, can lead to numbness of organs, muscle paralysis, breathing difficulties and even death in humans.[1–3] It can be accumulated by filter-feeding bivalves and fishes, and thus enter the food chain.[4] The oral lethal doses for humans is 5.7 μg kg^{-1}, therefore approximately 0.57 mg of saxitoxin is lethal if ingested and the lethal dose by injection is about 0.6 μg kg^{-1}. The human inhalation toxicity of aerosolized saxitoxin is estimated to be 5 mg min m^{-3}. It is suggested that saxitoxin can enter the body *via* open wounds and a lethal dose is 50 μg per person by this route. Moreover, saxitoxin is listed in schedule 1 of the Chemical Weapons Convention.[5] Thus, it is of great significance to accurately detect STX in drinking water and seafood to reduce the potential poisoning risks.

Currently, many techniques have been developed for recognition and analysis of trace STX including high performance liquid chromatography (HPLC),[6] enzyme-linked immunosorbent assays (ELISAs),[7] capillary electrophoresis (CE),[8] surface-enhanced Raman scattering (SERS),[9] and electrochemical biosensors.[10] However, HPLC and CE require sophisticated and expensive equipment, complex pretreatment, and skilful staff, thereby being too difficult for the detection of STX directly. SERS possesses poor sensitivity and specificity to poisons, and also needs advanced installation.[11] ELISA exhibits poor stability along with high cost and risk of false positive result.[12,13] In turn, electrochemical sensors are highly sensitive and demonstrate fast response and good stability, which makes them extensively used in the detection of various substances.[14] Meanwhile, the widespread application of electrochemical sensors is still limited by their unsatisfactory selectivity. Therefore, the development of highly selective electrochemical sensors to overcome these drawbacks is an urgent task.

Aptamers are selected *in vitro* functional short single-stranded DNA or RNA sequences (oligonucleotides) that have high affinities and specificities to target molecules, from small molecules to cells and tissues.[15,16] Typically, aptamers possess several important advantages, such as high selectivity and chemical stability, low cost, easy synthesis and modification.[17–19] Since their discovery in 1990, aptamers have been directly applied in biosensors for detection of various species[20–22] such as food toxins.[23,24] The aptamer to STX (APTSTX1) was first reported by Handy *et al.* in 2013.[25] However, the unsatisfactory binding affinity made the aptamer unsuitable for analytical application. Later, Zheng *et al.* generated the aptamer with a 30-fold higher affinity (M-30f).[26] Over time, this led to the emergence of diverse aptamer-based detection methods for STX.[27–29] For example, Hou *et al.* designed an electrochemical aptasensor modified with the STX aptamer and multiwalled carbon nanotubes/self-assembled monolayer (MWCNTs/SAM), in which methylene blue (MB) served as indicator for STX detection, providing the detection limit of 0.38 nM and good selectivity.[27] Ullah *et al.* developed an aptasensor using aptamer-modified MXene for STX detection, whose efficiency was assessed *via* capacitance–voltage and constant-capacitance measurements.[29] The detection range of

College of Light-Textile Engineering and Art, Anhui Agriculture University, Hefei, 230009, China. E-mail: zbli@ahau.edu.cn; Ljunzhang@ahau.edu.cn

† Electronic supplementary information (ESI) available. See https://doi.org/10.1039/d2ra03690h

the aptasensor was 1.0–200 nM and the detection limit was 0.03 nM. Park *et al.*[30] fabricated an electrochemical biosensor using round-type micro-gap electrodes as working electrode, and the sensitivity for STX detection was improved by introducing the porous platinum nanoparticle (pPtNP) that enhanced the electrochemical sensitivity. The biosensor has a detection limit of 4.669 pg mL^{-1} and a wide linear concentration range of 10 pg mL^{-1} to 1 μg mL^{-1}. Obviously, the realization of high sensitivity of these electrochemical aptasensors depends on nanomaterials. Can we achieve high sensitivity without using nanomaterials?

It is known that MB was often used as an electrochemical indicator to monitor reaction process in electrochemical studies. However, MB also has excellent electrocatalytic properties, which can efficiently improve electron transfer between analytes and electrodes.[31]

In this study, we developed a facile electrochemical sensor based on a short anti-STX aptamer with a methylene blue (MB) incorporated at the 3′-end (MB-Apt), in which MB was used to promote the electron transfer ability. The MB-Apt modified Au electrode served as the working electrode. Differential pulse voltammetry (DPV) was employed to evaluate the properties of the electrochemical aptasensor. In particular, the changes in the oxidation current were observed when STX reacted with the aptamer. This showed the ability of the proposed aptasensor to detect STX with high selectivity and sensitivity. Besides, the preparation conditions of the aptasensor were optimized to improve the current signal.

2. Experimental methods

2.1 Chemicals and reagents

The anti-saxitoxin aptamers used in this study were produced at Sangon Biotech Co., Ltd (Shanghai, China). Their sequences as follows: M-30f (5′-TTTTT TTG AGG GTC GCA TCC CGT GGA AAC AGG TTC ATT G-3′), HS-M-30f (HS-Apt: HS 5′-TTTTT TTG AGG GTC GCA TCC CGT GGA AAC AGG TTC ATT G-3′), aptamer modified with 3′-methylene blue (MB-Apt, HS 5′-TTTTT TTG AGG GTC GCA TCC CGT GGA AAC AGG TTC ATT G-3′ MB) and T5 (a short DNA strand containing 5 thymine bases) (HS 5′-TTTTT-3′).[32] Saxitoxins (STX), okadaic acid (OA), and neo-saxitoxin (neo-STX) were purchased from National Research Council of Canada. Tris(2-carboxyethyl) phosphine hydrochloride (TCEP) and tris(hydroxymethyl) aminomethane (Tris) were purchased from Sigma-Aldrich Sigma-Aldrich (USA, **https://www.sigmaaldrich.com**) and stored at 4 °C. Sodium chloride (NaCl), $K_3[Fe(CN)_6]/K_4[Fe(CN)_6]$ (1 : 1), hydrochloric acid (HCl, 37%), potassium chloride (KCl), magnesium chloride ($MgCl_2$), and ethyl alcohol were provided by Sinopharm Chemical Reagent Co., Ltd All the reagents were of analytical grade or better. Ultrapure water and a freshly prepared solution were used as well.

2.2 Fabrication of aptasensor and electrochemical measurements

The MB-Apt-modified Au electrode (ϕ3 mm) (MB-Apt/Au) served as the working electrode for the aptasensor. First, the gold electrode surface was polished with 1.0, 0.3 and 0.05 μm wet alumina powders successively, and then exposed to sequential cleaning using absolute ethyl alcohol and ultrapure water to remove pollutants. Subsequently, the gold electrode was immersed in a MB-Apt solution (0.5 μM, 10 mM Tris, 100 mM NaCl, 20 mM $MgCl_2$, 10 mM TCEP, pH 7.4) at 4 °C for 4 h to immobilize the MB-Apt through the formation of Au–S bonds. Finally, the electrode surface was carefully rinsed with 10 mM Tris–HCl (0.1 M NaCl, 0.02 mM $MgCl_2$) to eliminate the unbonded MB-Apt molecules.

Then, the surface of the MB-Apt/Au electrode was treated with 10 μL T5 solution (10 μM, 10 mM Tris, 100 mM NaCl, 20 mM $MgCl_2$, 10 mM TCEP, pH 7.4) at 4 °C for an hour to support the MB-Apt, causing MB away from the electrode surface. Finally, the electrode surface was carefully rinsed with 10 mM Tris–HCl to remove unbounded T5 and dried with nitrogen. The resulting T5/MB-Apt/Au electrode was denoted as STX electrochemical aptasensor and stored in the refrigerator at 4 °C for further use.

For the STX detection, 10 μL STX standard solutions of different concentrations (0, 1, 5, 10, 30, 100, 300, 500, 1000 nM) were dropped onto the surfaces of the above prepared electrodes which was then incubated for 30 min at 4 °C and rinsed with 10 mM Tris–HCl to remove unbounded STX.

The surface morphologies of Au and modified electrodes were evaluated by tapping-mode atomic force microscopy (AFM, Bruker, Germany). The AFM micrographs were afterwards processed using NanoScope Analysis software.

All electrochemical measurements were performed using a CHI660E electrochemical workstation (Shanghai Chen Hua Instrument Co., Ltd, China) in standard three electrode system, where Au electrode or modified Au electrode served as the working electrode, SCE (sat. KCl) and Pt wire served as reference and counter electrodes, respectively. Prior to cyclic voltammetry (CV), electrochemical impedance spectroscopy (EIS), and differential pulse voltammetry (DPV) studies, the electrodes were transferred to the electrochemical cell containing 1 mM $K_3[Fe(CN)_6]/K_4[Fe(CN)_6]$ with 0.1 M KCl. For the CV measurements, the potential window was ranged from −0.2 to 0.4 V at a scan rate of 50 mV S^{-1}. For the EIS experiments, the potential was set as 0.175 V, the frequency range was 0.1 Hz to 1 MHz, and the alternating potential was 10 mV. For the DPV measurements, the potential window was set as −0.2 to 0.6 V at a scan rate of 25 mV S^{-1}. After being removed from the solution, the electrodes were washed with ultrapure water to eliminate extraneous substances. All the experiments were carried out under ambient conditions.

3. Results and discussion

3.1 Principle of the electrochemical aptasensor

Scheme 1 illustrates the stepwise modification and the detection principle of the electrochemical aptasensor. First, MB-Apt, in which MB using as electron mediator to promote the electron transfer ability in the DPV sensing system, was immobilized onto the gold electrode *via* the gold-sulfur bonds. Subsequently, T5 was modified onto the MB-Apt/Au electrode to prevent MB-

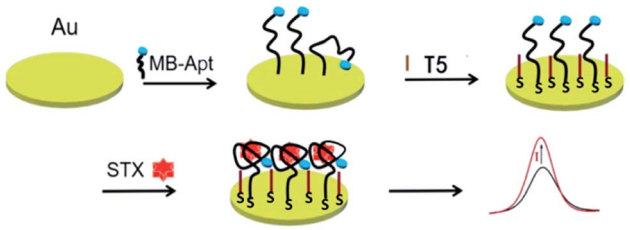

Scheme 1 The schematic diagram of an electrochemical aptasensor for saxitoxin detection, modified with anti-STX aptamer with methylene blue at the 3′-end (MB-Apt).

Apt from collapsing. In this way, MB molecules moved away from the electrode surface, which restricted the electron transfer from MB, resulting in a weak oxidation current. In the presence of STX, the aptamer MB-Apt would bind specifically to STX and form a folded conformation, bringing MB closer to the surface of electrode promoting electron transfer toward its surface, which resulting the oxidation current increased. As the change in the peak current relies on the concentration of STX, the aptasensor can be used to detect STX indirectly.

3.2 Characterizations of sensing interface

In order to evaluate the electrochemical characteristics of the modified electrodes during stepwise fabrication of the aptasensor and their detection capacity, the CV measurements were performed on the electrodes placed in 1 mM $[Fe(CN)_6]^{3-/4-}$ solution with 0.1 M KCl. The results are shown in Fig. 1a. In particular, a pair of clear reversible redox peaks is observed on the surface of a bare gold electrode, which decreased after the modification of the aptamer. Moreover, a drastic decrease in the redox peak intensity in the case of modified T5 suggests that T5 molecules not only occupied the excess binding sites, but also supported the collapsed aptamer keeping the MB far away from the electrode, which hinder the diffusion of $[Fe(CN)_6]^{3-/4-}$ molecules to the Au electrode surface. However, the peak current of the sensor has increased after incubation of the modified electrode with STX, which reflects the aptamers have successfully captured STX and folded into specific conformation structures to improve the electron transfer between $[Fe(CN)_6]^{3-/4-}$ and the Au substrate.

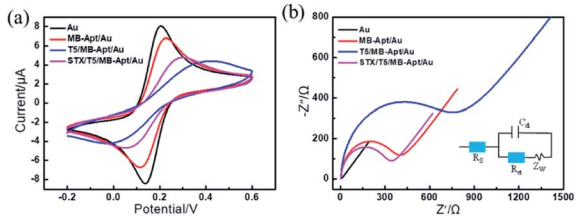

Fig. 1 (a) Cyclic voltammograms in 1 mM $K_3[Fe(CN)_6]/K_4[Fe(CN)_6]$ (1 : 1) solution containing 0.1 M KCl. Scan rate: 50 mV S^{-1}. (b) Nyquist diagrams for different electrodes at room temperature in 1 mM $K_3[Fe(CN)_6]/K_4[Fe(CN)_6]$ (1 : 1) solution containing 0.1 M KCl with the frequency range of 0.1 Hz to 1 MHz. Biasing potential: 0.175 V. Amplitude: 10 mV. The equivalent circuit used to fit the experimental impedance data is presented.

As a powerful tool for monitoring the interfacial properties of the electrode surface, electrochemical impedance spectroscopy (EIS) was employed to characterize the electron transfer resistance of different electrodes. The results are shown in Fig. 1b along with the equivalent circuit as the inset. The diameter of the semicircle in the EIS curves corresponds to the charge transfer resistance (R_{et}). It can be seen that the impedance of the bare-gold electrode is about 4 Ω, indicating that there was almost no charge transfer resistance on the electrode surface. After a step-by-step construction of MB-Apt and T5, the corresponding resistance values increased to 346 Ω and 662 Ω, respectively. Further, incubation of STX made R_{et} of the modified electrode decreased to 297 Ω, indicating that MB can efficiently improve electron transfer between analyses and electrodes. The CVs along with EIS results indicate that the electrochemical aptasensor was successfully constructed and can be used for STX detection.

To further confirm the successful grafting of MB-Apt on the surface of electrode, FTIR spectra was measured and listed in Fig. S1.† As shown in Fig. S1,† the peaks were observed at 3393 cm^{-1} may attributed to $-NH_2$, 1358 cm^{-1}, 664 cm^{-1} and 2936 cm^{-1} attributed to C–N vibration and heterocycle structure of MB-Apt, respectively.[33] The characteristic peak was observed at 1658 cm^{-1} attributed to the vibration of C=N of MB. The peaks at 1452 cm^{-1}, 1252 cm^{-1} and 1074 cm^{-1} may attributed to C–O, P–O and P=O. These results revealed the successful immobilization of the MB-Apt on the surface of electrode.

3.3 Morphology characterization of the sensing interface

To further analyze the morphology of the fabricated electrodes, atomic force microscope (AFM) was applied to examine the surface morphologies of Au, T5/MB-Apt/Au, and STX/T5/MB-Apt/Au electrodes. The corresponding results are given in Fig. 2. It is evident that the unmodified bare Au electrode possesses a smooth surface (Fig. 2a). However, fixing a certain amount of MB-Apt and T5 on the electrode surface *via* the Au–S bounds led to the average grain size and surface roughness of the electrode increased (Fig. 2b). Noticeably that, after STX is added, both the parameters increased significantly, indicating that the anti-STX aptamer (MB-Apt) successfully captured STX and folded it into a specific conformation structure.

3.4 Performance optimization of the aptasensor

To assess the performance of the proposed sensor, its experimental conditions including supporting electrolyte solution,

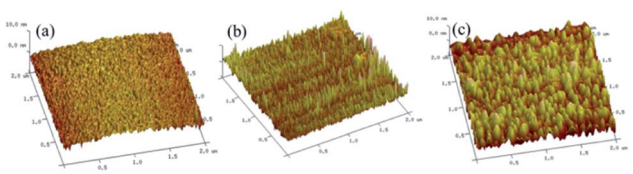

Fig. 2 3D atomic force microscopy images of (a) bare Au, (b) T5/MB-Apt/Au, and (c) STX T5/MB-Apt/Au electrode surfaces (the scan areas are 2 × 2 μm^2).

immobilization time, aptamer concentrations, concentration ratios between MB-Apt and T5, and adsorption time were thoroughly studied. The corresponding results are available in Fig. S2–S6 of ESI.†

Supporting electrolyte solution was one of the most important factors affecting the sensing properties of electrochemical aptasensor. In order to evaluate the effect of supporting electrolyte on the sensing ability of the aptasensor the electrochemical behavior of STX on the modified electrodes was investigated by cyclic voltammetry (−0.5 to 0.4 V) with 30 nM STX in 0.1 M PBS (pH = 7) and 1 mM $K_3[Fe(CN)_6]/K_4[Fe(CN)_6]$ solution. As shown in Fig. S2,† a weak peak current change at −0.32 V belongs to MB and a peak current at 0.15 V may be due to STX were observed in PBS. However, only a redox peak was at 0.16 V the electrode showed a current change about 4.2 μA when use 1 mM $K_3[Fe(CN)_6]/K_4[Fe(CN)_6]$ solution as supporting electrolyte. The above results demonstrated that the sensing ability of the aptasensor was better in 1 mM $K_3[Fe(CN)_6]/K_4[Fe(CN)_6]$ (1 : 1) solution. Therefore 1 mM $K_3[Fe(CN)_6]/K_4[Fe(CN)_6]$ (1 : 1) solution was chosen as supporting electrolyte.

To evaluate the effect of immobilization time of MB-Apt on the sensing ability of the aptasensor, 1 mM $K_3[Fe(CN)_6]/K_4[Fe(CN)_6]$ (1 : 1) solution containing 10 nM STX was selected as the supporting electrolyte and a temperature of 25 °C corresponded to the detection conditions. As shown in Fig. S3,† the change in the current (ΔI) of the aptasensor increased with increasing immobilization time of MB-Apt from 2 to 4 h, and then decreased when the immobilization time exceeded 4 h. In this respect, 4 h was chosen as the optimal MB-Apt modification time.

The concentration of MB-Apt was one of the most important factors affecting the sensing properties of the developed aptasensor. According to Fig. S4,† the value of ΔI reached its maximum at 0.5 μM, meaning that the optimum concentration of MB-Apt was 0.5 μM. The weaker signal response at higher MB-Apt concentrations could be due to the fact that excess aptamers were modified on the electrode surface, hindering the electron transfer.

To establish the optimum concentration ratios between the anti-STX aptamer and T5, the higher concentrations (2.5, 5, 10, 25, 50 μM) of the latter were added to 0.5 μM MB-Apt solution. As seen in Fig. S5,† the modified electrode had the maximum value of ΔI at a concentration of 10 μM of T5, that is the corresponding MB-Apt-to-T5 concentration ratio was 1 : 20. This indicates that 20 times shorter single-stranded T5 could just support the aptamer segments and achieve the best sensing performance.

After STX was added, the electrochemical signal (ΔI) of the modified electrode was monitored within a time period from 10 min up to 50 min. In particular, the value of ΔI of the modified electrode increased with the increase of the adsorption time of STX, and reached saturation within 30 min (Fig. S6†). Therefore, $K_3[Fe(CN)_6]/K_4[Fe(CN)_6]$ (1 : 1) solution was selected as supporting electrolyte, the modification time of 0.5 μM MB-Apt as 4 h, the relevant MB-Apt-to-T5 concentration ratio was 1 : 20, and the adsorption time of STX was 30 min.

3.5 Analytical performance of the aptasensor

The sensitivity and dynamic range of the electrochemical aptasensor were investigated by detecting DPV peaks at different concentrations of STX under the optimal conditions (Fig. 3). As can be observed from Fig. 3a, the DPV peaks of the sensor continuously increased with the increase of STX, which was due to the effective capture of STX by MB-Apt bringing MB closer to the surface of electrode promoting electron transfer toward its surface. Fig. 3b displays the corresponding calibration plots of the channel current change (ΔI) *versus* the STX concentration. The aptasensor is found to have a notable current response as a log-linear function of STX concentration with a correlation coefficient (R) of 0.9819 and sensitivity with a peak current change of 2.92 μA per decade is obtained within a range from 1 nM to 1 μM.

To further prove the sensitivity of the aptasensor, EIS was imployed to characterize the resistance values after incubation of different concentration of STX. The results were shown in Fig. S7.† As can be seen from Fig. S7,† the resistance values of the aptasensor were decreased significantly with the increase of STX, resulting from the effective capture of STX by MB-Apt, which are consistent with the DPV data. Therefore, it can be concluded that the electrochemical aptasensor can be used for sensitivity detection of STX.

The sensing performance of the T5 modified aptasensor was investigated as well, and the results are available in Fig. S8 (ESI†). Although the electrochemical signal decreased with the addition of STX, the parameter ΔI was not proportional to the STX concentration, and the ΔI was weaker than T5/MB-Apt modified sensor. This means that the sensing ability of the sensor modified with T5 is insufficient for the detection of STX. And the weak signal could be due to the attachment of STX to the electrode surface, thus hindering the electron transfer. As for the unmodified sensor, no obvious changes were observed in the DPV peaks (Fig. S9†).

The electrochemical aptasensor constructed in this work has higher detection range compared with other aptamer based sensors (Table 1). Moreover, compared with other electrochemical aptasensors, the electrochemical aptasensor has a wider linear range and similar detection limit without using any nano materials or nanostructures (Table 1), indicating that the simple electrochemical aptasensor prepared in this work can be used for the sensitivity detection of STX.

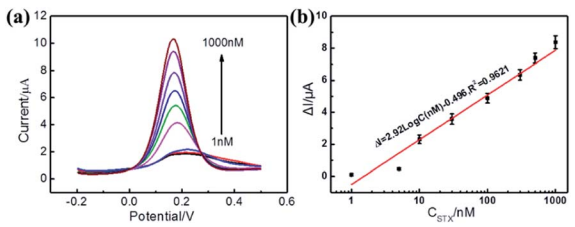

Fig. 3 (a) DPVs obtained for aptasensor after incubation with different concentrations of STX (0, 1, 5, 10, 30, 100, 300, 500, 1000 nM, respectively) in 1 mM $K_3[Fe(CN)_6]/K_4[Fe(CN)_6]$ (1 : 1) solution containing 0.1 M KCl. Scan rate: 25 mV S^{-1}. (b) The plot of DPV peaks changes (ΔI) *vs.* STX concentration.

Table 1 Analytical performance of different STX sensors

Methods	LOD	Linear range	Ref.
Electrochemical aptasensor	0.92 nM	1–400 nM	10
Electrochemical aptasensor	0.38 nM	0.9–30 nM	27
Electrochemical aptasensor	1.2 pg mL^{-1}	—	34
Electrochemical aptasensor	4.669 pg mL^{-1}	10 pg mL^{-1} to 1 μg mL^{-1}	30
Fluorescent aptasensor	10.0 nM	0–80.3 nM	32
SERS aptasensor	11.7 nM	10–200 nM	35
Colorimetric aptasensor	0.142 nM	0.145–37.3 nM	36
Colorimetric aptasensor	0.042 nM	0.078–2.5 nM	37
Electrochemical aptasensor	1 nM	1–1000 nM	This work

3.6 The selectivity of the electrochemical aptasensor for STX detection

The selectivity of the aptasensor to STX was investigated using neo-STX and okadaic acid (OA) as interference toxins. In turn, metal ions (K^+, Na^+, Ca^{2+}, Mg^{2+}, and Fe^{3+}) commonly found in the water environment were selected as interferers. The selectivity of the sensor was evaluated by measuring its DPV peaks. Under the same experimental conditions, 30 nM STX, OA, and neo-STX were added respectively, and the concentration of metal ions was 100 nM. The results are shown in Fig. 4. The aptasensor exhibited the highest current response with a ΔI value of 3.6 μA at a STX concentration of 30 nM. However, the ΔI values at adding 30 nM of neo-STX (0.81 μA) and OA (0.87 μA) were considerably lower than those obtained in the presence of STX. Meanwhile, the current responses to 100 nM of K^+, Na^+, Ca^{2+}, Mg^{2+}, and Fe^{3+} were quite low, with the values of ΔI less than 0.16 μA. It can thus be concluded that the designed electrochemical aptasensor is highly selective to STX. In particular, the change of DPV peaks of the aptasensor is found to be induced by the adsorption of STX molecules by the anti-STX aptamer MB-Apt, as well as the electrocatalysis of MB. In other words, the selectivity of the aptamer-modified electrochemical sensor is accomplished through the specific molecular recognition of STX by the aptamer.

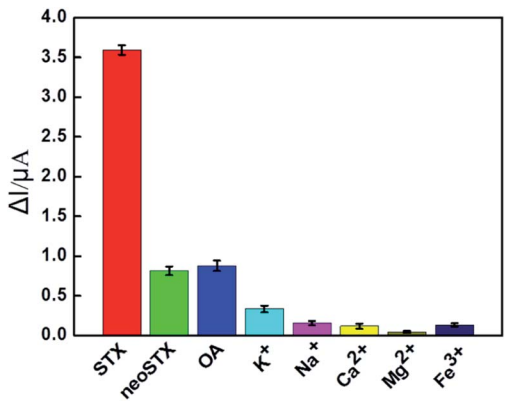

Fig. 4 Comparison of relative current responses (ΔI) in the presence of different toxins and metal ions at different concentration (toxins: 30 nM, common metal ions: 100 nM). Error bars represent standard deviations from three independent measurements.

3.7 Reproducibility of the electrochemical aptasensor

The reproducibility of the electrochemical aptasensor was investigated using five T5/MB-Apt/Au electrodes as the working electrodes of the electrochemical aptasensors; T5/MB-Apt/Au electrodes were independently fabricated by similar procedures. As shown in Table S1,† the obtained relative standard deviation (RSD) was 8.50% for a STX concentration of 10 nM, indicative of good reproducibility of the fabrication.

3.8 Real sample analysis

In order to evaluate the practical performance of the electrochemical aptasensor, the constructed sensor was applied for the direct analysis of STX in the shellfish samples purchased in the market. Shellfish was washed carefully to remove sediment pollutants. Then the shellfish was boiled with HCl solution (0.1 M) for 5 minutes and was centrifuged at 3500 rpm for 10 minutes. Free STX was spiked in shellfish, samples to achieve a final concentration of 3, 10, and 30 nM. Differential pulse voltammetry was carried out for the detection of STX. Table S2† shows the analysis result of these samples. The RSDs were less than 9.8%, and the recoveries of STX ranged from 84% to 112%. Therefore, the prepared the electrochemical aptasensor can be applied for the detection of STX in real samples.

4. Conclusions

In this study, a simple electrochemical sensor modified with anti-STX aptamer was successfully used as a STX sensor. In this sensor, MB was used to promote the electron transfer ability and the aptamer was covalently bounded to the electrode surface. The electrochemical sensor was shown to dramatically improve the sensitivity because of the electrocatalysis of MB. Meanwhile, the anti-STX aptamer MB-Apt remarkably improved the selectivity of the sensor because of the specific binding of

the aptamer, making the latter fold into a specific conformation. The optimized aptasensor exhibited a high sensitivity with a peak current change of 2.92 μA per decade within a STX concentration range from 1 nM to 1000 nM and a LOD of 1 nM. Furthermore, the electrochemical sensor modified with MB-Apt could recognize STX from interference toxins and common metal ions.

Conflicts of interest

The authors declare no competing financial interest.

Acknowledgements

This work was supported by the Natural Science Foundation of Anhui Province, China (Grant no.1908085QB89, 2008085MC84) and the Natural Science Foundation of the Anhui Higher Education Institutions of China (Grant no. KJ2021A0131, KJ2021A0132).

References

1 A. P. Thottumkara, W. H. Parsons and J. D. Bois, Saxitoxin, *Angew. Chem., Int. Ed.*, 2014, **53**(23), 5760–5784.
2 A. Capper, L. J. Flewelling and K. Arthur, Dietary exposure to harmful algal bloom (HAB) toxins in the endangered manatee (Trichechus manatus latirostris) and green sea turtle (Chelonia mydas) in Florida, USA, *Harmful Algae*, 2013, **28**, 1–9.
3 V. M. Bricelj, L. Connell, K. Konoki, S. P. MacQuarrie, T. Scheuer, W. A. Catterall and V. L. Trainer, Sodium channel mutation leading to saxitoxin resistance in clams increases risk of PSP, *Nature*, 2005, **434**(7034), 763–767.
4 S. Cheng, B. Zheng, D. B. Yao, S. L. Kuai, J. J. Tian, H. J. Liang and Y. S. Ding, Study of the binding way between saxitoxin and its aptamer and a fluorescent aptasensor for detection of saxitoxin, *Spectrochim. Acta, Part A*, 2018, **204**, 180–187.
5 **https://en.wikipedia.org/wiki/Saxitoxin**.
6 F. M. Van Dolah, S. E. Fire, T. A. Leighfield, C. M. Mikulski and G. J. Doucette, Determination of paralytic shellfish toxins in shellfish by receptor binding assay: collaborative study, *J. AOAC Int.*, 2012, **95**(3), 795–812.
7 R. E. Wharton, M. C. Feyereisen, A. L. Gonzalez, N. L. Abbott, E. I. Hamelin and R. C. Johnson, Quantification of saxitoxin in human blood by ELISA, *Toxicon*, 2017, **133**, 110–115.
8 A. S. A. Keyon, R. M. Guijt, A. Gaspar, A. A. Kazarian, P. N. Nesterenko, C. J. Bolch and M. C. Breadmore, Capillary electrophoresis for the analysis of paralytic shellfish poisoning toxins in shellfish: comparison of detection methods, *Electrophoresis*, 2014, **35**(10), 1496–1503.
9 C. T. Cao, P. Li, H. G. Liao, J. P. Wang, X. H. Tang and L. B. Yang, Cys-functionalized AuNP substrates for improved sensing of the marine toxin STX by dynamic surface-enhanced Raman Spectroscopy, *Anal. Bioanal. Chem.*, 2020, **412**, 4609–4617.
10 X. Y. Qi, X. C. Yan, L. H. Zhao, Y. F. Huang, S. Wang and X. G. Liang, A facile label-free electrochemical aptasensor constructed with nanotetrahedron and aptamer-triplex for sensitive detection of small molecule: Saxitoxin, *J. Electroanal. Chem.*, 2020, **858**, 113805.
11 X. Jin, J. L. Chen, X. X. Zeng, L. J. Xu, Y. N. Wu and F. F. Fu, A signal-on magnetic electrochemical immunosensor for ultra-sensitive detection of saxitoxin using palladium-doped graphitic carbon nitride-based non-competitive strategy, *Biosens. Bioelectron.*, 2019, **128**, 45–51.
12 S. Sato, Y. Takata, S. Kondo, A. Kotado, N. Hogo and M. Kodama, Quantitative ELISA kit for paralytic shellfish toxins coupled with sample pretreatment, *J. AOAC Int.*, 2014, **97**(2), 339–344.
13 M. H. Kim and S. J. Choi, Immunoassay of paralytic shellfish toxins by moving magnetic particles in a stationary liquid-phase lab-on-a-chip, *Biosens. Bioelectron.*, 2015, **66**, 136–140.
14 C. L. Justino, A. C. Freitas, R. Pereira, A. C. Duarte and T. R. Santos, Recent developments in recognition elements for chemica sensors and biosensors, *Trends Anal. Chem.*, 2015, **68**, 2–17.
15 A. D. Ellington and J. W. Szostak, In vitro selection of RNA molecules that bind specific ligands, *Nature*, 1990, **346**(6287), 818–822.
16 I. Alvarez-Martos and E. E. Ferapontova, Electrochemical label-free aptasensor for specific analysis of dopamine in serum in the presence of structurally related neurotransmitters, *Anal. Chem.*, 2016, **88**(7), 3608–3616.
17 Z. A. Carter and R. Kataky, A G-quadruplex aptamer based impedimetric sensor for free lysine and arginine, *Sens. Actuators, B*, 2017, **243**, 904–909.
18 D. X. Yang, X. C. Liu, Y. Y. Zhou, L. Luo, J. C. Zhang, A. Q. Huang, Q. M. Mao, X. Chen and L. Tang, Aptamer-based biosensors for detection of lead(II) ion: a review, *Anal. Methods*, 2017, **9**(13), 1976–1990.
19 G. Mayer, The chemical biology of aptamers, *Angew. Chem., Int. Ed.*, 2009, **48**(15), 2672–2689.
20 X. J. Chen, Y. G. Pan, H. Q. Liu, X. J. Bai, N. Wang and B. Zhang, Label-free detection of liver cancer cells by aptamer-based microcantilever biosensor, *Biosens. Bioelectron.*, 2016, **79**, 353–358.
21 K. Ling, H. Y. Jiang, Y. Li, X. J. Tao, C. Qiu and F. R. Li, A self-assembling RNA aptamer-based graphene oxide sensor for the turn-on detection of theophylline in serum, *Biosens. Bioelectron.*, 2016, **86**, 8–13.
22 H. M. Meng, H. Liu, H. L. Kuai, R. Z. Peng, L. T. Mo and X. B. Zhang, Aptamer-integrated DNA nanostructures for biosensing, bioimaging and cancer therapy, *Chem. Soc. Rev.*, 2016, **45**(9), 2583–2602.
23 E. Shimaa, N. Andy, S. Mohamed and M. Z. Mohamed, Label-free voltammetric aptasensor for the sensitive detection of microcystin-LR using graphene-modified electrodes, *Anal. Chem.*, 2014, **86**(15), 7551–7557.
24 X. J. Du, D. Jing, H. A. Li, N. Hao, T. Y. You and K. Wang, An intriguing signal-off responsive photoelectrochemical aptasensor for ultrasensitive detection of microcystin-LR and its mechanism study, *Sens. Actuators, B*, 2018, **259**, 316–324.

25 S. M. Handy, B. J. Yakes, J. A. DeGrasse, K. Campbell, C. T. Elliott, K. M. Kanyuck and S. L. Degrasse, First report of the use of a saxitoxin-protein conjugate to develop a DNA aptamer to a small molecule toxin, *Toxicon*, 2013, **61**, 30–37.

26 X. Zheng, B. Hu, S. X. Gao, D. J. Liu, M. J. Sun, B. H. Jiao and L. H. Wang, A saxitoxin-binding aptamer with higher affinity and inhibitory activity optimized by rational site-directed mutagenesis and truncation, *Toxicon*, 2015, **101**, 41–47.

27 L. Hou, L. S. Jiang, Y. P. Song, Y. H. Ding, J. H. Zhang, X. P. Wu and D. P. Tang, Amperometric aptasensor for saxitoxin using a gold electrode modified with carbon nanotubes on a self-assembled monolayer, and methylene blue as an electrochemical indicator probe, *Microchim. Acta*, 2016, **183**(6), 1971–1980.

28 H. J. Gu, L. L. Hao, H. Ye, P. F. Ma and Z. P. Wang, Nuclease-assisted target recycling signal amplification strategy for graphene quantum dot-based fluorescent detection of marine biotoxins, *Microchim. Acta*, 2021, **188**(4), 118.

29 N. Ullah, W. Chen, B. Noureen, Y. L. Tian, L. P. Du, C. S. Wu and J. Ma, An electrochemical Ti_3C_2Tx aptasensor for sensitive and label-free detection of marine biological toxins, *Sensors*, 2021, **21**(14), 4938.

30 J. A. Park, N. Kwon, E. Park, Y. H. Kim, H. J. Jang, J. H. Min and T. Lee, Electrochemical biosensor with aptamer/porous platinum nanoparticle on round-type micro-gap electrode for saxitoxin detection in fresh water, *Biosens. Bioelectron.*, 2022, **210**, 114300.

31 S. Su, Q. Hao, Z. Y. Yan, R. M. Dong, R. Yang, D. Zhu, J. Chao, Y. Zhou and L. H. Wang, A molybdenum disulfide@Methylene Blue nanohybrid for electrochemical determination of microRNA-21, dopamine and uric acid, *Microchim. Acta*, 2019, **186**, 607.

32 S. Cheng, B. Zheng, D. B. Yao, S. Kuai, J. J. Tian, H. J. Liang and Y. S. Ding, Study of the binding way between saxitoxin and its aptamer and a fluorescent aptasensor for detection of saxitoxin, *Spectrochim. Acta, Part A*, 2018, **204**, 180–187.

33 J. Chi, M. Chen, L. Deng, X. Lin and Z. Xie, A facile AuNPs@aptamer modified mercaptosiloxane-based hybrid affinity monolith with an unusually high coverage density of aptamer for on-column selective extraction of ochratoxin A, *Analyst*, 2018, **143**, 5210–5217.

34 X. Jin, J. L. Chen, X. X. Zeng, L. J. Xu, Y. N. Wu and F. F. Fu, A signal-on magnetic electrochemical immunosensor for ultra-sensitive detection of saxitoxin using palladium-doped graphitic carbon nitride-based non-competitive strategy, *Biosens. Bioelectron.*, 2019, **128**, 45–51.

35 S. Cheng, B. Zheng, D. B. Yao, Y. Wang, J. J. Tian, L. H. Liu, H. J. Liang and Y. S. Ding, Determination of saxitoxin by aptamer-based surface-enhanced raman scattering, *Anal. Lett.*, 2019, **52**(6), 902–918.

36 L. Li, Y. L. Zhao, X. C. Yan, X. Y. Qi, L. L. Wang, R. Ma, S. Wang and X. Z. Mao, Development of a terminal-fixed aptamer and a label-free colorimetric aptasensor for highly sensitive detection of saxitoxin, *Sens. Actuators, B*, 2021, **344**, 130320.

37 Y. L. Zhao, L. Ling, R. Ma, L. L. Wang, X. C. Yan, X. Y. Qi, S. Wang and X. Z. Mao, A competitive colorimetric aptasensor transduced by hybridization chain reaction-facilitated catalysis of AuNPs nanozyme for highly sensitive detection of saxitoxin, *Anal. Chim. Acta*, 2021, **1173**, 338710.